2013

3D Micron-scale Imaging of the Cortical Bone Canal Network in Human Osteogenesis Imperfecta (OI)

John R. Jameson
Marquette University

Carolyne Albert
Marquette University, carolyne.albert@marquette.edu

Bjoern Busse
University Medical Center, Hamburg

Peter A. Smith
Marquette University

Gerald F. Harris
Marquette University, gerald.harris@marquette.edu

3D micron-scale imaging of the cortical bone canal network in human osteogenesis imperfecta (OI)

John R. Jameson[a,b,c], Carolyne I. Albert[b,c,d], Bjoern Busse[e], Peter A. Smith[c,d], Gerald F. Harris[b,c,d]

[a]Advanced Light Source, Lawrence Berkeley National Lab, 1 Cyclotron Rd., Berkeley, CA, USA 94720; [b]Dept. of Biomedical Engineering, Marquette University, 1250 W. Wisconsin Ave., Milwaukee, WI, USA 53233; [c]Orthopaedic & Rehabilitation Engineering Center (OREC), Marquette University, 735 N. 17th St., ASF 105, Milwaukee, WI, USA 53233; [d]Shriners Hospitals for Children, 2211 N. Oak Park Ave., Chicago, IL, USA 60707; [e]Dept. of Osteology & Biomechanics, University Medical Center, Hamburg-Eppendorf, Lottestr. 59, D-22529 Hamburg, Germany

ABSTRACT

Osteogenesis imperfecta (OI) is a genetic disorder leading to increased bone fragility. Recent work has shown that the hierarchical structure of bone plays an important role in determining its mechanical properties and resistance to fracture. The current study represents one of the first attempts to characterize the 3D structure and composition of cortical bone in OI at the micron-scale. A total of 26 pediatric bone fragments from 18 individuals were collected during autopsy (N_c=5) or routing orthopaedic procedures (N_{OI}=13) and imaged by microtomography with a synchrotron light source (SRμCT) for several microstructural parameters including cortical porosity (*Ca.V/TV*), canal surface to tissue volume (*Ca.S/TV*), canal diameter (*Ca.Dm*), canal separation (*Ca.Sp*), canal connectivity density (*Ca.ConnD*), and volumetric tissue mineral density (*TMD*). Results indicated significant differences in all imaging parameters between pediatric controls and OI tissue, with OI bone showing drastically increased cortical porosity, canal diameter, and connectivity. Preliminary mechanical testing revealed a possible link between cortical porosity and strength. Together these results suggest that the pore network in OI contributes greatly to its reduced mechanical properties.
Keywords: Osteogenesis imperfecta, brittle bone disease, micro-computed tomography, synchrotron, cortical porosity, bone microstructure, strength, pediatric bone

1. INTRODUCTION

Osteogenesis imperfecta (OI), or brittle bone disease, is the most common genetic bone disorder, affecting approximately 1:10,000 persons.[1] OI is generally characterized by mutations that lead to reduced quantity and/or quality of type I collagen and its associated structural proteins. Collagen is an important organic constituent of many organ systems throughout the body, and it is the most ubiquitous protein in animals.[2] As a result, symptoms in OI vary widely but can include a host of problems including brittle bones, spine deformities,[3] impaired lung function,[3] and heart valve abnormalities,[4] among others. Because of this heterogeneity, patients are generally classified into one of a growing number of clinical groups (Table 1). However, in practice it is difficult to distinguish between types VI-VIII in children on the basis of clinical or radiological features. Of the remaining groups, types I, IV, and III are the most commonly studied, and these three types provide a good framework for comparing characteristics of mild, moderate, and severe OI, respectively.

Until recently, the prevailing paradigm for assessing bone strength has been that changes in the loading environment affect bone remodeling and mineralization, which in turn directly influence mechanical properties.[5] However, bone is a composite of flexible collagen and brittle hydroxyapatite mineral, and as such its properties depend not only on the composition but also on the structure or organization of the tissue. Cortical bone has a highly complex, hierarchical structure (Figure 1) that is often difficult or impractical to assess in patients because the resolution of *in vivo* imaging

techniques is limited. The radiation dose of X-ray based methods is also of particular concern in pediatric OI patients, who routinely undergo X-rays for fractures and surgical planning.

Table 1. Clinical classification of OI patients (Adapted from Van Dijk, et al[6]). *Denotes types included in the current study.

Clinical type	Severity	Affected gene (and associated protein)
I*	Mild (non-deforming)	COL1A1/2 (type I collagen)
II	Lethal (perinatal)	COL1A1/2 (type I collagen)
III*	Severe	COL1A1/2 (type I collagen)
IV*	Moderate	COL1A1/2 (type I collagen)
V	Moderate	Unknown
VI	Moderate/severe	Unknown
VII	Moderate	CRTAP (cartilage associated protein)
VIII	Severe/lethal	LEPRE1 (leucine proline-enriched proteoglycan)

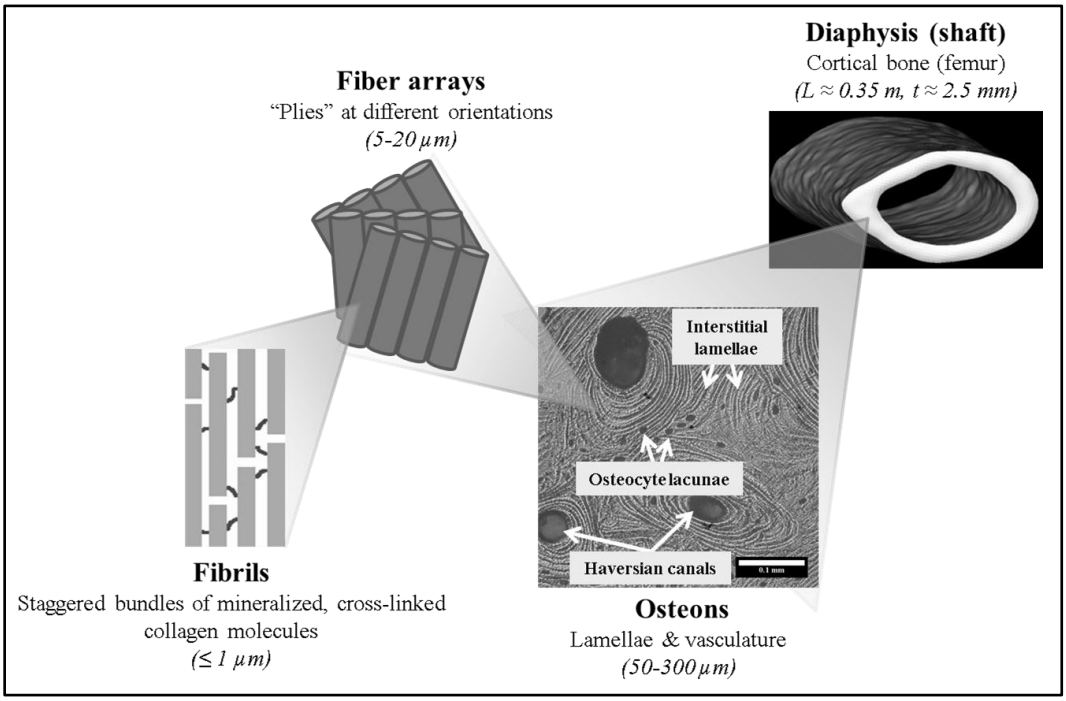

Figure 1. Hierarchical structure of cortical bone (with associated length scales).

The emergence of *ex vivo* imaging techniques such as micro-computed tomography (μCT) for biomedical applications has made it possible to explore small structures (*e.g.*, osteons, osteocyte lacunae, vasculature, etc.) in the interior of bone at a vastly improved level of resolution. Continuous advances in computational power have enabled complex analysis of bone porosity using direct 3D measurements that do not rely on stereological or material distribution assumptions. Although the availability of synchrotron user facilities is low (and the demand for beamtime high), these systems provide an ideal tool for visualizing the micron-scale characteristics of bone.[7] The vast majority of fractures in OI occur in the long bones of the arms and legs (*i.e.*, femur, tibia, humerus, radius). The purpose of this study was therefore to characterize porosity and composition in small, clinically relevant fragments from the mid-diaphysis of long bones. A secondary aim was to explore possible relationships between OI bone structure, mineralization, and strength.

2. METHODS

2.1 Study population

Pediatric patients with OI often require corrective surgeries and osteotomies that yield small bone fragments, which would normally be discarded post-operatively or saved for histological analysis. After obtaining written consent/assent and IRB approval (Rush University Medical Center #10101309 and Marquette University #HR-2176), we collected 21 such fragments from the femur, tibia, and humerus of 13 children with OI. We also collected 5 specimens from pediatric controls due to autopsy (LBL BUA#205). Table 2 summarizes relevant donor information. All specimens were stored fresh-frozen until just prior to testing.

Table 2. Study population. *Note: N=total number of donors, n=total number of specimens.

	Control (N_c=5, n=5)	**OI (N_{OI}=13, n=21)**
Phenotype	All healthy (no known musculoskeletal disease)	Mild (type I): n=4 Moderate (type IV): n=5 Severe (type III): n=12
Age, years [interquartile range]	7 [3-11]	10 [8-12]
Gender	All female	Male: n=10 Female: n=11
Anatomical location	All femur	Femur: n=8 Tibia: n=11 Humerus: n=2

2.2 Synchrotron radiation µCT (SRµCT) imaging

All bone fragments were imaged (continuous mode, 1025 projections, 180° rotation) on the tomography beamline at the Advanced Light Source (BL 8.3.2, Berkeley, CA) using a monochromatic X-ray energy of 17 keV. To reduce phase contrast effects and improve resolution, we used the beamline's newly commissioned Optique Peter X-ray microscope (Lentilly, France), which allows for closer (*i.e.*, <5mm) scintillator-to-objective distances. This system, along with the other relevant beamline hardware and software, has been described previously.[8] A combination of the 4x and 10x objective lenses was used, with resulting nominal pixel sizes of 1.7 µm and 0.6 µm, respectively. After flat field correction, subsequent reconstructions were performed using a filtered back projection algorithm in Octopus commercial software (Octopus 8.6, inCT, Ghent, Belgium) to generate scaled, 16-bit TIF stacks. The linear scaling equation was embedded in the header file so that floating point gray values could be recovered for composition measurements.

2.3 K_2HPO_4 tissue phantom

Hydroxyapatite (HA) solutions have commonly been used as tissue phantoms to create calibration curves relating the reconstructed gray values (which represent the linear attenuation coefficient, µ, of a material) to known mineral concentrations.[12] However, the resolution of SRµCT is fine enough to detect small inhomogeneities in these solutions, and recent work has shown that dipotassium hydrogen phosphate (K_2HPO_4) solutions provide better results.[13] A stock solution of K_2HPO_4 was therefore prepared in nanopure water and diluted to create the following concentrations (g K_2HPO_4/cm^3): 0, 200, 400, 800, 1000. A small amount of each solution was placed in thin-walled glass capillary tubes (SiO_2, t=0.5 mm) and imaged in a similar manner to above. The resulting calibration curve is shown in Figure 2.

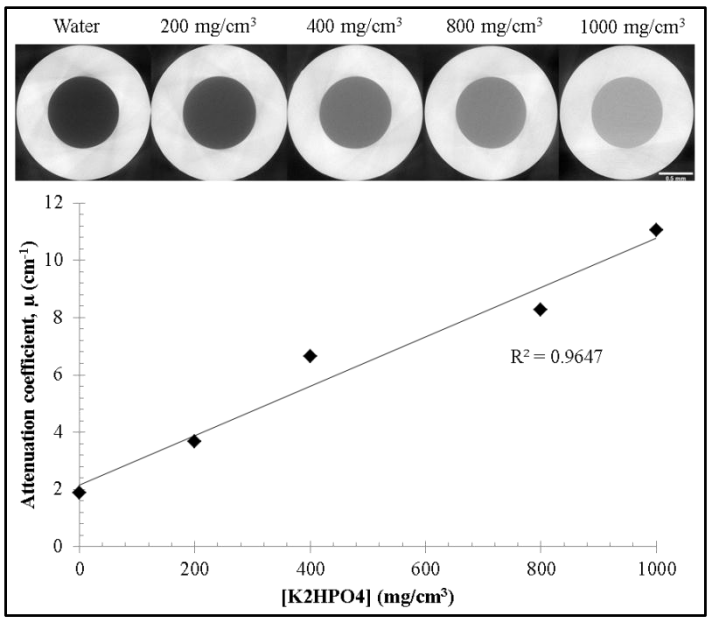

Figure 2. Bone phantom calibration curve. Each data point corresponds to the image above.

2.4 Microstructural and composition measurements

All reconstructed data sets were analyzed and visualized using the open-source software suite Fiji, a distribution of ImageJ.[14] Regions of interest (ROIs) were selected along a 1-mm section of each image stack. After filtering each ROI using a 3D bilateral filtering algorithm,[9] segmentation was performed using the built-in iterative IsoData thresholding algorithm[10] on the stack histogram. The pore structure was separated into canals and osteocyte lacunae using the Particle Analyser algorithm in Fiji.

Microstructural parameters were then measured using BoneJ,[11] a set of customizable plugins for Fiji. Table 3 shows a list of all parameters calculated, along with physical descriptions for each parameter. 3D methods for calculating canal diameter (*Ca.Dm*) and canal separation (*Ca.Sp*) were based on maximum inscribed sphere algorithms; consequently, processing time was highly dependent on the size of the image features. To maximize computational efficiency, we downsampled each ROI prior to performing these measurements.

Compositional measurements require accurate, quantitative analysis of image gray values. Therefore we converted the images back to their floating point values and segmented in a similar manner to above. Each ROI was then analyzed to determine the average gray value of all voxels that had been segmented as bone. Using the calibration curve generated from the different concentrations of the K_2HPO_4 bone phantom (Figure 2), this average gray value was converted to a volumetric tissue mineral density (*TMD*, in g/cm^3).

Table 3. Summary of cortical bone microstructural parameters.

Microstructural parameter	Units	Description
Cortical porosity, *Ca.V/TV*	%	Volume of all haversian and Volkmann's canals, including any additional void space (excluding osteocyte lacunae and canaliculi), divided by the total ROI volume
Canal surface to tissue volume, *Ca.S/TV*	mm^{-1}	Total surface area of the pore network (calculated using a marching cubes algorithm) divided by the total ROI volume
Canal diameter, *Ca.Dm*	µm	Average diameter of all voids (calculated using a maximum inscribed sphere algorithm)
Canal separation, *Ca.Sp*	µm	Average distance between voids (calculated using a maximum inscribed sphere algorithm)
Canal connectivity density, *Ca.ConnD*	mm^{-3}	Number of connected structures in the pore network (calculated using the Euler characteristic) divided by the total ROI volume

2.5 Pilot mechanical testing

To determine whether porosity is an important factor affecting bone strength, we tested a subset of the specimens to failure in either three-point bending or tension. A total of 10 beams were machined, 5 each from control and severe (type III) OI, using a low-speed diamond saw under constant water irrigation. Beams were machined such that the direction of osteons was aligned parallel to the long axis of the beam. OI beams were tested to failure using a customized 3-point bending jig attached to a materials testing frame (Instron, Model 3345, Norwood, MA),[15] while control beams were tested using a custom-made tensile rig (Omega, LC703-10).[16] The two groups were tested under different loading conditions because they were to be included in other related work. To ensure physiologically relevant strength results, all beams remained hydrated throughout testing. The resulting load versus displacement curves were normalized to create stress versus strain curves, where the strength was defined as the maximum stress achieved before failure.

2.6 Statistics

For the microstructural and compositional imaging data, the OI specimens were pooled and compared to the control population using a Mann Whitney U test with a significance level of 0.05. Linear correlations were also calculated to investigate possible relationships between the microstructural, compositional, and strength results.

3. RESULTS

3.1 Microstructural & compositional results

OI bone displayed statistically significant ($p<0.05$) differences across all microstructural measurements (Table 4). There was an increase in cortical porosity (7x), canal surface to tissue volume (2x), canal diameter (3x), and canal connectivity density (8x) for the OI bone compared to controls. The range of values for each parameter was much higher in OI bone compared to controls, indicating a high degree of heterogeneity in the pore network. There were no obvious trends between the different types of OI bone. The volume renderings in Video 1 show representative pore networks for each experimental group. Although there does appear to be a consistent orientation of pores parallel to the direction of osteons, the OI network shows higher variability and generally appears more isotropic than controls. There was no apparent correlation between cortical porosity and tissue mineral density in the OI group. There was, however, a strong negative correlation ($R^2=0.92$) between these two parameters in pediatric controls.

Table 4. Microstructural & compositional results summary. All values listed as median [interquartile range]. *****Denotes $p<0.05$ between pediatric controls and OI (pooled).

Parameter	Pediatric controls	OI (pooled)	Mild OI (type I)	Moderate OI (type IV)	Severe OI (type III)
Cortical porosity, *Ca.V/TV* (%)	3.3 [3.0-3.4]	21.1* [14.4-23.4]	22.9 [19.0-26.3]	14.4 [13.5-23.4]	19.7 [15.8-22.7]
Canal surface to tissue volume, *Ca.S/TV* (mm^{-1})	3.0 [2.8-3.1]	6.2* [5.4-8.2]	7.7 [6.2-9.3]	5.5 [4.0-7.3]	6.1 [5.6-8.3]
Canal diameter, *Ca.Dm* (µm)	41 [29-42]	126* [102-137]	107 [101-116]	130 [101-133]	131 [119-149]
Canal separation, *Ca.Sp* (µm)	195 [177-197]	253* [215-333]	175 [148-338]	335 [301-435]	249 [219-311]
Canal connectivity density, *Ca.ConnD* (mm^{-3})	8.5 [2.5-14.9]	67.7* [39.7-126.5]	151.9 [87.3-252.3]	61.2 [20.0-101.6]	67.7 [50.5-97.9]
Tissue mineral density, *TMD* (g/cm^3)	3.6 [3.6-3.7]	2.5* [2.4-2.7]	2.8 [2.7-2.9]	2.3 [2.3-2.4]	2.5 [2.4-2.6]

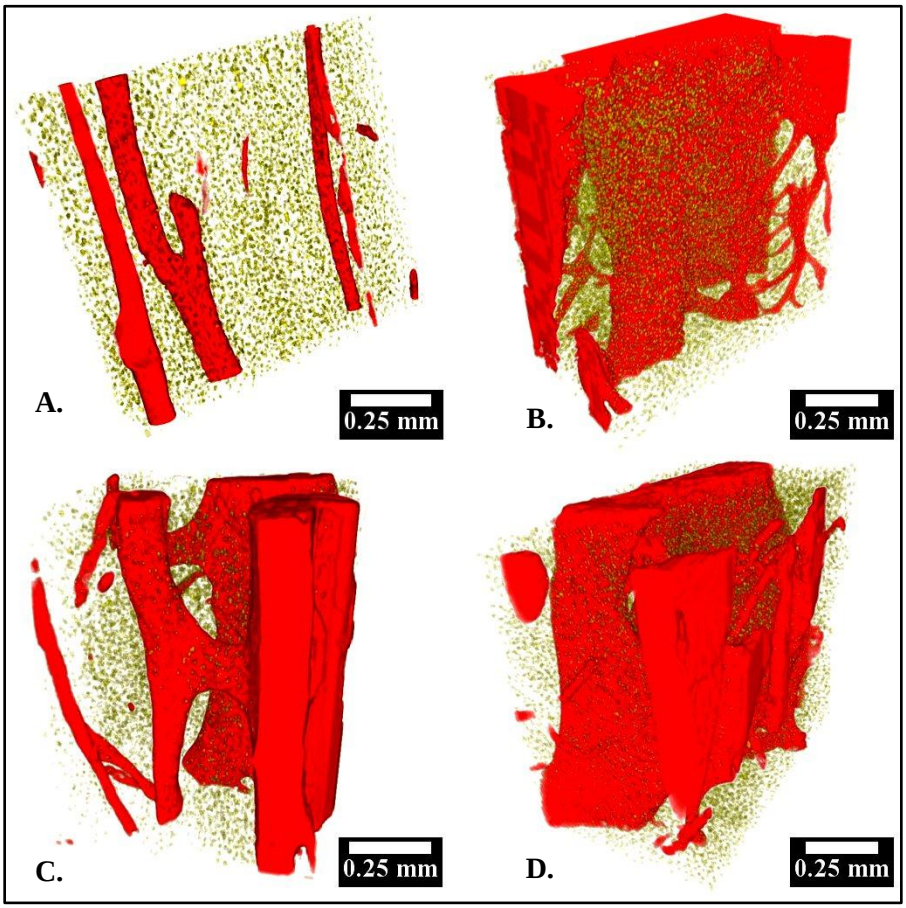

Video 1. Comparison of cortical bone pore network (red=pores, yellow=osteocyte lacunae). A: Pediatric controls; B: Mild (type I) OI; C: Moderate (type IV) OI; D: Severe (type III) OI. *Note: Osteocyte lacunae shown for reference but not included in porosity calculations. For colorized video, see online version of paper: http://dx.doi.org/doi.number.goes.here

3.2 Preliminary mechanical results

Initial results from bending tests indicated a correlation between cortical porosity and flexural strength in severe OI bone (Figure 3). There was no apparent correlation between these parameters in the control group. Median strength values for the control and OI groups tested in tension and bending, respectively, were 94 MPa and 76 MPa. However, since these groups were tested under different experimental conditions, they should not be compared directly.

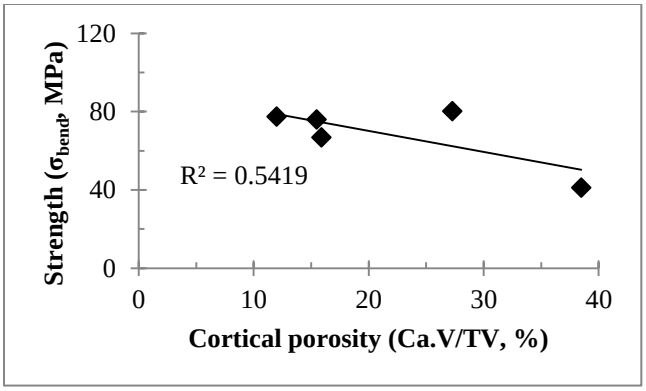

Figure 3. Correlation between cortical porosity and strength in severe OI.

4. DISCUSSION/CONCLUSIONS

Although bone structure is an important determinant of mechanical properties, to date there is very little data examining this topic in the OI literature. Several histological studies have reported on the cortical wall thickness at the iliac crest.[17-19] The most extensive of these analyzed 70 pediatric biopsies from mild, moderate, and severe OI patients, finding marked cortical thinning across all types.[19] It is unclear how well these measurements translate to other skeletal sites such as the long bones, which are the most common fracture locations (and thus the most clinically relevant regions in assessing fracture risk) in OI patients. One recent study used high-resolution peripheral quantitative computed tomography (HR-pQCT) to analyze bone composition and structure *in vivo* at the ultradistal radius and ultradistal tibia in adult patients with mild (type I) OI.[20] The study reported decreases in OI volumetric bone mineral density and several trabecular parameters; however, the resolution was too low (≈80 μm) to analyze the entire canal network. Alternatively, SRμCT is well-suited for capturing the 3D, micron-scale properties of the bone tissue and canal network.[7] This is significant because recent work on the effects of aging has shown that microstructural features such as haversian canals play an important role in resisting fracture.[21] The purpose of the current study was to characterize the cortical bone pore network in mild (type I), moderate (type IV), and severe (III) OI, as well as to compare these groups to a pediatric control population.

We observed drastic increases in porosity, canal diameter, and canal connectivity across all OI types. Whereas bone tissue from the control group displayed a highly oriented canal network, OI bone was much more heterogeneous, with large fluctuations in canal diameter and organization. These characteristics should impair bone strength, as large, connected pores offer little resistance to crack propagation. Indeed, preliminary mechanical property data reflected this relationship with structure, as there appeared to be a negative correlation between cortical porosity and strength in severe OI bone. These results warrant an expanded study to investigate the relative importance of porosity in determining strength.

The effect of OI severity was not readily noticeable in our analysis, as both microstructural and compositional measures were similar between the three groups. Although not statistically significant, the fact that mild (type I) OI bone showed the highest cortical porosity of the three groups is surprising. A total of 11 of the 13 OI donors (including all of the type I donors) in this study had been treated with bisphosphonates, which alter mineral metabolism by reducing the activity of bone-resorbing osteoclasts. Differences in the dosage and frequency of drug administration could help explain some of

the pore network variability between the OI groups. A recent nanoindentation study revealed that tissue level elastic modulus (a measure of material stiffness) was approximately 7% higher in mild (type I) versus moderate and severe OI.[22] These findings suggest that there may be material level adaptations in mild OI bone that allow it to be stronger than the other types despite higher porosity. To investigate this possibility, future work is needed combining detailed drug history information with pore network analysis, as well as local mineralization and materials testing.

Overall compositional results were mixed, as we found a strong inverse correlation between cortical porosity and volumetric tissue mineral density in the control group, but not in OI. This observation is interesting because previous studies have shown a correlation between mineral measurements and bone volume fraction (*BV/TV*, a corollary to cortical porosity) in trabecular OI bone.[23] Bone turnover is elevated in OI[19], and in general turnover is higher in trabecular versus cortical bone.[24] Together these findings point to fundamental differences in bone modeling/remodeling between these two types of bone.

Because it is often difficult to obtain and test human OI bone specimens, mouse models have become a useful surrogate for understanding the disease and evaluating potential treatment therapies. A recent pilot study on the *oim* model of severe OI found an increase in the number of canals and osteocyte lacunae in diseased mice versus controls.[25] The researchers suggested that the increase in the number of pores in *oim* bone may help explain the reduced fracture resistance of this tissue. In contrast with our results, the study did not observe increased canal size or cortical porosity in diseased bone. There are fundamental differences between the microstructure of murine versus human bone that could explain this phenomenon (*e.g.*, murine cortical bone does not contain osteons). In light of our current findings, a more detailed study on *oim* bone is warranted to determine whether there are common characteristics in the pore network between these species.

In summary, this study presents some of the first data on the 3D characteristics of the cortical bone pore network in mild, moderate, and severe OI. We report significant increases in cortical porosity, canal diameter, and canal connectivity in OI bone compared to a pediatric control group. Preliminary mechanical studies indicate a possible correlation between cortical porosity and mechanical strength in OI bone. Future studies focusing on pore architectural characteristics such as canal orientation, canal branching, and degree of anisotropy will shed further light on the effect of bone microstructure on mechanical properties. Together this information will be valuable in understanding the cause of bone fragility in OI, as well as in developing and evaluating new treatment strategies.

ACKNOWLEDGEMENTS

The contents of this proceedings paper were developed with support from an Advanced Light Source (ALS) doctoral fellowship, in cooperation with a grant from the Department of Education, NIDRR grant number H133E100007. However, the contents do not necessarily represent the policy of the Department of Energy or the Department of Education, and you should not assume endorsement by the Federal Government. JJ graciously acknowledges the beamline scientists at the ALS, Dr. Dula Parkinson and Dr. Alastair MacDowell, for their assistance in collecting and analyzing the synchrotron data. JJ also recognizes Dr. Robert Ritchie and Dr. Elizabeth Zimmerman of the Materials Science Division at Lawrence Berkeley National Lab (Berkeley, CA) for access to the strength data for the pediatric control group.

REFERENCES

[1] Royce, P.M., Steinmann, B., [Connective Tissue and Its Heritable Disorders: Molecular, Genetic, and Medical Aspects], John Wiley & Sons Publishing, New York, 385-430 (2002).
[2] Lodish, H., Berk, A., Zipursky, S.L. [Molecular Cell Biology], W.H. Freeman Publishers, New York, Section 22.3 (2000).
[3] Widmann, R.F., Bitan, F.D., Laplaza, J., Burke, S.W., DiMaio, M.F., Schneider, R., "Spinal deformity, pulmonary compromise, and quality of life in osteogenesis imperfecta," Spine 24(16), 1673-1678 (1999).
[4] Stein, D., Kloster, F.E., "Valvular heart disease in osteogenesis imperfecta," Am Heart J 94(5), 637-641 (1977).

[5] Frost, H.M., “Skeletal structural adaptations to mechanical usage (SATMU): 1. Redefining Wolff’s law: The bone modeling problem,” The Anatomical Record 226(4), 403-413 (1990).
[6] Van Dijk, F.S., Pals, G., Van Rijn, R.R., Nikkels, P.G.J., Cobben, J.M., “Classification of osteogenesis imperfecta revisited,” European Journal of Medical Genetics 53(1), 1-5 (2010).
[7] Bousson, V., Peyrin, F., Bergot, C., Hausard M., Sautet, A., Laredo, J.D., “Cortical bone in the human femoral neck: Three-dimensional appearance and porosity using synchrotron radiation,” J Bone Miner Res 19(5), 794-801 (2004).
[8] MacDowell, A.A., Parkinson, D.Y., Haboub, A., Schaible, E., Nasiatka, J.R., Yee, C.A., Jameson, J.R., Ajo-Franklin J.B., Broderson, C.R., McElrone, A.J., “X-ray micro-tomography at the advanced light source,” Proc SPIE 8506, 850618-1-850618-14 (2012).
[9] Ushizima, D., Bianchi, A., de Bianchi, C., Wes Bethel, E., “Material science image analysis using Quant-CT in ImageJ,” ImageJ User and Developer Conference 2012, Mondorf-les-Bains,Luxembourg (2012). Ridler, T.W., &
[10] Calvard, S., "Picture thresholding using an iterative selection method", IEEE Transactions on Systems, Man and Cybernetics 8(8), 630-632 (1978).
[11] Doube, M., Kłosowski, M. M., Arganda-Carreras, I., Cordeliéres, F., Dougherty R. P., Jackson, J., Schmid, B., Hutchinson, J. R., Shefelbine, S. J., “BoneJ: free and extensible bone image analysis in ImageJ,” Bone 47(6), 1076-1079 (2010).
[12] Salome´, M., Peyrin, F., Cloetens, P., Odet, C., Laval-Jeantet, A. M., Baruchel, J., Spanne, P., “A synchrotron radiation microtomography system for the analysis of trabecular bone samples,” Med Phys 26(10), 2194-2204 (1999).
[13] Nuzzo, S., Peyrin F., Cloetens, P., Baruchel, J., Boivin, G., “Quantification of the degree of mineralization of bone in three dimensions using synchrotron radiation microtomography,” Med Phys 29(11), 2672-2681 (2002).
[14] Schneider, C. A., Rasband, W. S., Eliceiri, K. W., “NIH Image to ImageJ: 25 years of image analysis,” Nature Methods 9(7), 671-675 (2012).
[15] Albert, C.I., Jameson, J., Harris, G., “Design and validation of bending test method for characterization of miniature pediatric bone specimens,” Proc IMechE Part H: J Engineering in Medicine 227(2), 105-113 (2013).
[16] Zimmerman, E. A., Schaible, E., Bale, H., Barth, H. D., Tang, S. Y., Reichert, P., Busse, B., Alliston, T., Ager III, J. W., Ritchie, R. O., “Age-related changes in the plasticity and toughness of human cortical bone at multiple length scales,” Proc Natl Acad Sci USA 108(35), 14416-14421 (2011).
[17] McCarthy, E.F., Earnest, K., Rossiter, K., Shapiro, J., “Bone histomorphometry in adults with type IA osteogenesis imperfecta,” Clin Orthop 336, 254-262 (1997).
[18] Ste-Marie, L.G., Charhon, S.A., Edouard, C., Chapuy, M.C., Meunier, P.J., “Iliac bone histomorphometry in adults and children with osteogenesis imperfecta,” J Clin Pathol 37, 1081-1089 (1984).
[19] Rauch, F., Travers, R., Parfitt, A.M., Glorieux, F.H., “Static and dynamic bone histomorphometry in children with osteogenesis imperfecta,” Bone 26(6), 581-589 (2000).
[20] Folkestad, L, Hald, J.D., Hansen, S., Gram, J., Langdahl, B., Abrahamsen, B., Brixen, K., “Bone geometry, density, and microarchitecture in the distal radius and tibia in adults with osteogenesis imperfecta type I assessed by high-resolution pQCT,” J Bone Miner Res 27(6), 1405-1412 (2012).
[21] Koester, K.J., Ager III, J.W., Ritchie, R.O., “The true toughness of human cortical bone measured with realistically short cracks,” Nature Materials 7, 672-677 (2008).
[22] Albert, C., Jameson, J., Toth, J.M., Smith, P., Harris, G., “Bone properties by nanoindentation in mild and severe osteogenesis imperfecta,” Clin Biomech 28(1), 110-116 (2013).
[23] Jameson, J., Albert C., Smith, P., Molthen, R., Harris, G., “Micro-CT characterization of human trabecular bone in osteogenesis imperfecta,” Proc SPIE 7965, 79650I-1-79650I-8(2011).
[24] Clark, B., “Normal bone anatomy and physiology,” Clin J Am Soc Nephrol 3, S131-S139 (2008).
[25] Carriero, A., Doube, M., Levchuk, A., Schneider, P., Muller, R., Shefelbine, S.J., “Cortical tissue porosity of brittle osteogenesis imperfecta bone,” Proc ORS, 2206 (2011).